Journal of Molecular and Cellular Cardiology 105 (2017) 49–58

Contents lists available at ScienceDirect

Journal of Molecular and Cellular Cardiology

journal homepage: www.elsevier.com/locate/yjmcc

Membrane potential determines calcium alternans through modulation of SR Ca^{2+} load and L-type Ca^{2+} current

Giedrius Kanaporis *, Lothar A. Blatter *

Department of Physiology and Biophysics, Rush University Medical Center, Chicago, IL 60612, USA

ARTICLE INFO

Article history:
Received 4 November 2016
Received in revised form 2 February 2017
Accepted 26 February 2017
Available online 28 February 2017

Keywords:
Action potential
Alternans
Arrhythmia
Ca^{2+} signaling
Excitation-contraction coupling

ABSTRACT

Alternans is a risk factor for cardiac arrhythmia, including atrial fibrillation. At the cellular level alternans is observed as beat-to-beat alternations in contraction, action potential (AP) morphology and magnitude of the Ca^{2+} transient (CaT). It is widely accepted that the bi-directional interplay between membrane voltage and Ca^{2+} is crucial for the development of alternans, however recently the attention has shifted to instabilities in cellular Ca^{2+} handling, while the role of AP alternation remains poorly understood. This study provides new insights how beat- to-beat alternation in AP morphology affects occurrence of CaT alternans in atrial myocytes.

Pacing-induced AP and CaT alternans were studied in rabbit atrial myocytes using combined Ca^{2+} imaging and electrophysiological measurements. To determine the role of AP morphology for the generation of CaT alternans, trains of two voltage commands in form of APs recorded during large and small alternans CaTs were applied to voltage-clamped cells. APs of longer duration (as observed during small amplitude alternans CaT) and especially beat-to-beat alternations in AP morphology (AP alternans) reduced the pacing frequency threshold and increased the degree of CaT alternans. AP morphology contributes to the development of CaT alternans by two mechanisms. First, the AP waveform observed during small alternans CaTs coincided with higher end-diastolic sarcoplasmic reticulum Ca^{2+} levels ($[Ca^{2+}]_{SR}$), and AP alternans resulted in beat-to-beat alternations in end-diastolic $[Ca^{2+}]_{SR}$. Second, L-type Ca^{2+} current was significantly affected by AP morphology, where the AP waveform observed during large CaT elicited L-type Ca^{2+} currents of higher magnitude and faster kinetics, resulting in more efficient triggering of SR Ca^{2+} release.

In conclusion, alternation in AP morphology plays a significant role in the development and stabilization of atrial alternans. The demonstration that CaT alternans can be controlled or even prevented by modulating AP morphology has important ramifications for arrhythmia prevention and therapy strategies.

1. Introduction

Cardiac alternans is linked causally to cardiac arrhythmias, including atrial fibrillation [1–4], and sudden cardiac death [5–7]. At the cellular level cardiac alternans is observed as periodic beat-to-beat variation in contraction amplitude, action potential (AP) morphology and cytosolic Ca^{2+} transient (CaT) amplitude at constant stimulation frequency.

The strong correlation between AP and CaT alternans was demonstrated at whole heart and single cell levels [8,9], and it is generally agreed that the relationship between cytosolic Ca^{2+} concentration ($[Ca^{2+}]_i$) and membrane potential (V_m) plays a key role for the generation of alternans. While it is still debated whether disturbances of V_m or $[Ca^{2+}]_i$ regulation are the primary cause of alternans (summarized e.g. in [10,11]), growing evidence indicates that alternans is initiated by disturbances of intracellular Ca^{2+} handling [8,12–15]. The demonstration that CaT alternans can be elicited in voltage-clamped myocytes without beat-to-beat variation in V_m [8,15,16] provided strong evidence that AP alternation is not an absolute requirement for CaT alternans to occur, and instabilities of Ca^{2+} handling that lead to alternans are an inherent property of the cardiac myocytes. However, these observations cannot rule out a role of beat-to-beat alternations of membrane voltage dynamics for the development of cardiac alternans. The main support for V_m as an important contributor to alternans comes from computational cardiomyocyte models [17–19]. Because of the complexity of the bi-directional coupling between V_m dynamics and intracellular Ca^{2+} handling the experimental distinction between effects of Ca^{2+} and V_m is complicated and therefore experimental data on how AP morphology affects development of CaT alternans is scarce.

Abbreviations: AP, action potential; AP_{CaT_Large}, AP recorded during a large amplitude alternans Ca^{2+} transient; AP_{CaT_Small}, AP recorded during a small amplitude alternans Ca^{2+} transient; APD, action potential duration; AR, alternans ratio; $[Ca^{2+}]_{SR}$, SR Ca^{2+} concentration; CaT, Ca^{2+} transient; CICR, Ca^{2+}-induced Ca^{2+} release; ECC, excitation-contraction coupling; I_m, membrane current; LCC, L-type Ca^{2+} channel; NCX, Na^+/Ca^{2+} exchanger; SR, sarcoplasmic reticulum; V_m,, membrane potential.

* Corresponding authors at: Department of Physiology and Biophysics, Rush University Medical Center, 1750 W. Harrison Street, Chicago, IL 60612, USA.
E-mail addresses: Giedrius_Kanaporis@rush.edu (G. Kanaporis), Lothar_Blatter@rush.edu (L.A. Blatter).

http://dx.doi.org/10.1016/j.yjmcc.2017.02.004
0022-2828/

Most of the research on the mechanisms of alternans was performed in ventricular myocytes and tissue. In contrast, the interplay between V_m and Ca^{2+} in the atria and its ramification for atrial alternans remains poorly investigated despite the known connection between alternans and cardiac arrhythmia and the fact that atrial fibrillation is the most common cardiac rhythm disorder. Recently we have demonstrated that in atrial myocytes disturbances in Ca^{2+} cycling are a leading cause for the development of alternans, and alternans can be suppressed when release of Ca^{2+} from the sarcoplasmic reticulum (SR) is blocked [8]. However, these findings did not exclude the possibility that V_m dynamics also play an important role in the generation of alternans. Therefore, in this study we set out to determine the effects of alternating AP morphology on intracellular Ca^{2+} handling and the development of alternans in atria. In summary, here we demonstrate that, while beat-to-beat disturbances of cellular Ca^{2+} handling are the main cause for the development of cardiac alternans, both AP morphology and beat-to-beat alternations in AP dynamics play an important role in modifying the onset and degree of CaT alternans by affecting diastolic SR Ca^{2+} load and kinetics of L-type Ca^{2+} current (I_{LCC}).

2. Methods

2.1. Myocyte isolation

Atrial myocytes were isolated from male New Zealand White rabbits (~2.5 kg; Harlan Laboratories, Indianapolis, IN, USA). All procedures and protocols were approved by the Institutional Animal Care and Use Committee of Rush University and comply with the Guide for the Care and Use of Laboratory Animals of the National Institutes of Health. Rabbits were anaesthetized with an intravenous injection of sodium pentobarbital (100 mg/kg) and heparin (1000 UI/kg). Hearts were excised, mounted on a Langendorff apparatus and retrogradely perfused via the aorta. After an initial 5 min perfusion with oxygenated Ca^{2+}-free Tyrode solution (in mM: 140 NaCl, 4 KCl, 10 D-glucose, 5 Hepes, 1 $MgCl_2$, 10 BDM, 1000 UI/l Heparin; pH 7.4 with NaOH), the heart was perfused with minimal essential medium Eagle (MEM) solution containing 20 μM Ca^{2+} and 22.5 μg/ml Liberase TH (Roche Diagnostic Corporation, Indianapolis, IN, USA) for ~20 min at 37 °C. The left atrium was dissected from the heart and minced, filtered and washed in a MEM solution containing 50 μM Ca^{2+} and 10 mg/ml bovine serum albumin. Isolated cells were washed and kept in MEM solution with 50 μM Ca^{2+} at room temperature (20–24 °C) and were used within 1–8 h after isolation.

2.2. Solutions and experimental conditions

The standard Tyrode external solution was composed of (in mM): 135 NaCl, 5 KCl, 2 $CaCl_2$, 1 $MgCl_2$, 10 Hepes, 10 D-glucose; pH 7.4 with NaOH. All chemicals and reagents were from Sigma-Aldrich (St. Louis, MO, USA), unless otherwise stated. All experiments were performed at room temperature (20–24 °C).

2.3. Electrophysiological measurements

Electrophysiological signals were recorded from single cardiac myocytes in the whole-cell ruptured patch clamp configuration using an Axopatch 200A patch clamp amplifier, the Axon Digidata 1440A interface and pCLAMP 10.2 software (Molecular Devices, Sunnyvale, CA). Current and AP recordings were low-pass filtered at 5 kHz and digitized at 10 kHz.

For patch clamp experiments pipettes (1.5–3 MΩ filled with internal solution) were pulled from borosilicate glass capillaries (WPI, Sarasota, FL, USA) with a horizontal puller P-97 (Sutter Instruments, Novato, CA, USA) and filled with internal solution containing (in mM): 130 K^+ glutamate, 10 NaCl, 10 KCl, 0.33 $MgCl_2$, 4 MgATP, and 10 Hepes with pH adjusted to 7.2 with KOH. For simultaneous $[Ca^{2+}]_i$ measurements 100 μM Fluo-4 pentapotassium salt or Indo-1 pentapotassium salt (both fluorescent probes from Molecular Probes/Thermo Fisher Scientific, Waltham, MA) was added to the internal solution. Internal solutions were filtered through 0.22-μm pore filters. For AP measurements the whole-cell 'fast' current clamp mode of the Axopatch 200A was used and APs were evoked by 4 ms stimulation pulses with a magnitude ~1.5–2 times higher than AP activation threshold. V_m measurements were corrected for a junction potential error of −10 mV.

For AP clamp experiments voltage commands in form of atrial APs were generated from averages of APs (3 consecutive APs/cell) recorded from three individual cells paced at 1.3 Hz and exhibiting CaT alternans (Fig. 1). These representative AP waveforms were used in all AP voltage clamp experiments. Thus, the AP voltage commands were not specific for an individual cell and therefore are expected to differ marginally from the endogenous AP of a specific cell. Two voltage commands were generated: AP_{CaT_Large} representing APs recorded during large CaTs, and AP_{CaT_Small}, the AP-waveform observed during small CaTs. These two distinct AP waveforms were used to generate the following pacing protocols: 1) same-shape AP_{CaT_Large} protocol consisting of 24 consecutive AP_{CaT_Large} waveforms; 2) same-shape AP_{CaT_Small} protocol consisting of 24 consecutive AP_{CaT_Small} waveforms and 3) alternans AP protocol consisting of 12 consecutive AP_{CaT_Large}-AP_{CaT_Small} pairs. Stimulation frequency was modified by changing diastolic intervals between AP voltage commands. For statistical analysis of CaTs properties and CaT alternans only the last 6 CaTs elicited by the pacing protocol were analyzed to ensure that recordings were done at steady-state conditions.

L-type Ca^{2+} current (I_{LCC}) was measured as nifedipine (100 μM) sensitive current during AP clamp experiments under conditions where all other currents were blocked. K^+ currents were suppressed by the replacing all K^+ ions with Cs^+ in both extracellular and intracellular solutions, Cl^- channels were blocked with 300 μM 4,4′-diisothiocyanatostilbene-2,2′-disulfonic acid (DIDS), and Na^+/Ca^{2+} exchange (NCX) and Na^+ currents were eliminated by replacing all extracellular and intracellular Na^+ with tetraethylammonium (TEA). An agar salt bridge (1 M KCl) was used to minimize potential shifts during bath solution changes.

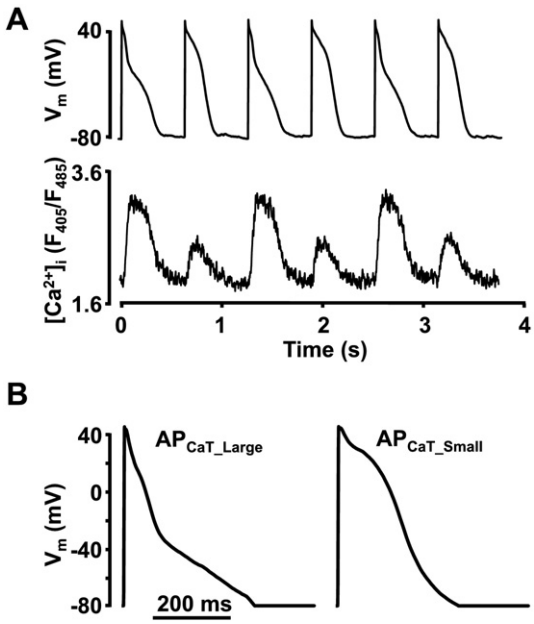

Fig. 1. Simultaneous CaT and AP alternans recording. A, Simultaneous recordings of APs and $[Ca^{2+}]_i$ from a single atrial myocyte under current clamp conditions and loaded with Indo-1. B, Typical AP waveforms recorded during large (AP_{CaT_Large}) and small (AP_{CaT_Small}) alternans CaTs used as voltage commands to pace cells during AP voltage clamp experiments.

2.4. Cytosolic and SR $[Ca^{2+}]$ measurements

2.4.1. Cytosolic $[Ca^{2+}]_i$

$[Ca^{2+}]_i$ was monitored simultaneously with APs (current clamp mode) or membrane currents (I_m; AP voltage clamp mode). For $[Ca^{2+}]_i$ measurements cells were loaded with fluorescent probes Fluo-4 pentapotassium salt (100 μM) or Indo-1 pentapotassium salt (100 μM) via the patch pipette. Fluo-4 fluorescence was excited at 485 nm with a xenon arc lamp and $[Ca^{2+}]_i$-dependent Fluo-4 signals were collected at 515 nm using a photomultiplier tube. Background-subtracted fluorescence emission signals (F) were normalized to resting fluorescence (F_0) recorded under steady-state conditions at the beginning of an experiment, and changes of $[Ca^{2+}]_i$ are presented as changes of F/F_0. Indo-1 fluorescence was excited at 357 nm (Xe arc lamp) and emitted cellular fluorescence was recorded simultaneously at 405 nm (F_{405}) and 485 nm (F_{485}) with photomultiplier tubes. F_{405} and F_{485} signals were background subtracted and changes of $[Ca^{2+}]_i$ are expressed as changes of the ratio F_{405}/F_{485}. Data recording and digitization were achieved using the Axon Digidata 1440A interface and pCLAMP 10.2 software. Fluorescence signals were low-pass filtered at 50 Hz.

2.4.2. SR $[Ca^{2+}]$ and SR Ca^{2+} load

For SR $[Ca^{2+}]$ ($[Ca^{2+}]_{SR}$) measurements myocytes were loaded with Fluo-5N/AM (10 μM; Molecular Probes/Thermo Fisher Scientific) for 90 min at 37 °C followed by washout (>20 min) in Tyrode solution. Fluo-5N fluorescence was excited at 485 nm with a Xe arc lamp and collected at 515 nm using a photomultiplier tube. Background-subtracted fluorescence emission signals (F) were normalized to resting fluorescence (F_0) recorded under steady-state conditions at the beginning of an experiment, and changes of $[Ca^{2+}]_{SR}$ are presented as changes of F/F_0. In addition to the Fluo-5N measurements SR Ca^{2+} load was determined with two additional approaches: 1) measurement of the $[Ca^{2+}]_i$ amplitude elicited with rapid application of caffeine (10 mM), and 2) as the integral of the NCX current recorded during the caffeine application.

2.4.3. CaT alternans

CaT alternans was induced by incrementally increasing the pacing frequency until stable alternans was observed. The degree of Ca^{2+} alternans was quantified as the alternans ratio (AR). $AR = 1 - [Ca^{2+}]_{i,Small} / [Ca^{2+}]_{i,Large}$, where $[Ca^{2+}]_{i,Large}$ and $[Ca^{2+}]_{i,Small}$ are the amplitudes of the large and small CaTs from a pair of alternating CaTs. By this definition AR values fall between 0 and 1, where $AR = 0$ indicates no Ca^{2+} alternans and $AR = 1$ indicates a situation where SR Ca^{2+} release is completely abolished on every other beat. CaTs were considered alternating when the beat-to-beat variation in CaT amplitude exceeded 10% ($AR > 0.1$) [8]. The amplitude of a CaT was measured as the difference in F_{405}/F_{485} or F/F_0 measured immediately before the stimulation pulse and the peak of the CaT.

2.5. Data analysis and presentation

Results are presented as individual observations or as mean ± SEM, and n represents the number of individual cells. Statistical significance was evaluated using unpaired and paired Student's *t*-test and differences were considered significant at $p < 0.05$.

3. Results

3.1. AP morphology affects intracellular Ca^{2+} release and generation of CaT alternans

To determine how AP morphology affects intracellular Ca^{2+} release in atrial myocytes $[Ca^{2+}]_i$ measurements were conducted under AP voltage clamp conditions. To generate AP voltage command signals, CaT and V_m were recorded first under current clamp conditions during pacing-induced CaT alternans (Fig. 1). Fig. 1A shows a sequence of CaTs and APs with beat-to-beat alternating morphology. Fig. 1B shows the two representative AP waveforms recorded in current clamp experiments during CaT alternans that were used for all subsequent AP clamp experiments as voltage commands. AP_{CaT_Large} refers to the AP recorded during the large amplitude alternans CaT, whereas AP_{CaT_Small} was recorded during the small amplitude alternans CaT. During AP clamp experiments cells were stimulated with the following pacing protocols: (i) same-shape AP_{CaT_Large} protocol; (ii) same-shape AP_{CaT_Small} protocol; and (iii) alternans AP protocol. First, the effect of the two AP waveforms on CaTs properties was analyzed at lower pacing frequency (1.19 Hz) that did not exhibit CaT alternans when paced with same-shape AP protocols (Fig. 2A). To ensure steady-state conditions, only the last six CaTs recorded at the end of the pacing protocol (consisting of a total of 24 stimuli) were included in the statistical analysis. CaTs elicited with the same-shape AP_{CaT_Small} were 18 ± 2% larger in magnitude (Fig. 2B and C) compared to CaT induced by the same-shape AP_{CaT_Large} protocol ($n = 17$). Interestingly, when the alternans AP protocol was applied at the same pacing frequency CaT alternans were induced (i.e. the pacing threshold for alternans decreased) and a reversal of the CaT amplitude-AP morphology relationship was observed. Now Ca^{2+} release of larger magnitude (by 17 ± 3%, $n = 16$) was elicited with the AP_{CaT_Large} voltage command (Fig. 2B and C). Furthermore, the AP waveform also affected the time to 80% of the CaT peak ($t_{80\%\_peak}$). The mean $t_{80\%\_peak}$ recorded during the same-shape AP_{CaT_Large} protocol (54.5 ± 3.3 ms, $n = 17$), was significantly shorter ($p < 0.0005$) than during same-shape AP_{CaT_Small} protocol (73.5 ± 5.4 ms, $n = 17$). The same tendency remained when cells were stimulated with the alternans AP protocol: $t_{80\%\_peak}$ was 57.1 ± 2.8 and 68.2 ± 5.1 ms ($p < 0.01$, $n = 16$) for AP_{CaT_Large} and AP_{CaT_Small}, respectively.

An increase in pacing frequency led to the development of CaT alternans also with the same-shape AP clamp protocols. Fig. 3A demonstrates a typical course of alternans development during the same-shape and alternans AP clamp protocols (all traces were recorded from the same atrial myocyte). Same-shape AP_{CaT_Small} protocols elicited CaT alternans at lower pacing frequency and with larger alternans ratio (AR, defined as $1 - [Ca^{2+}]_{i,Small} / [Ca^{2+}]_{i,Large}$, where $[Ca^{2+}]_{i,Large}$ and $[Ca^{2+}]_{i,Small}$ are the amplitudes of the large and small CaTs from a pair of alternating CaTs.) than the same-shape AP_{CaT_Large} protocol. The alternans AP clamp protocols further increased the degree of CaT alternans and lowered the pacing threshold where CaT alternans occurred (summarized in Fig. 3B). These data clearly demonstrate that AP morphology plays an important role for modulating intracellular Ca^{2+} release. AP morphology affects the threshold frequency for CaT alternans induction and determines the degree of CaT alternans. Furthermore, beat-to-beat alternation in AP waveform further contributes to the severity of CaT alternans.

3.2. In-phase and out-of-phase CaT and AP alternans

In the next set of the experiments we investigated factors that determine whether AP and CaT alternans are in-phase or out-of-phase during alternans AP clamp. Here, “in-phase” refers to the situation where a large CaT coincides with AP_{CaT_Large} and a small CaT is recorded with AP_{CaT_Small} during the alternans AP clamp segment of the protocol. In contrast, “out-of-phase” refers to a large CaT coinciding with AP_{CaT_Small} and the subsequent small CaT coinciding with AP_{CaT_Large}. In these series of experiments the pacing protocols were combined: either one of the two same-shape AP pacing protocols was immediately followed by the alternans AP protocol and cells were stimulated at a rate that induced stable CaT alternans during the preceding same-shape AP clamp protocol. At the transition from the same-shape AP to the alternans AP protocol two scenarios are possible: CaT alternans enter the alternans AP clamp pacing phase being “in-phase” or “out-of-phase” with the AP clamp voltage command. Fig. 4 illustrates the

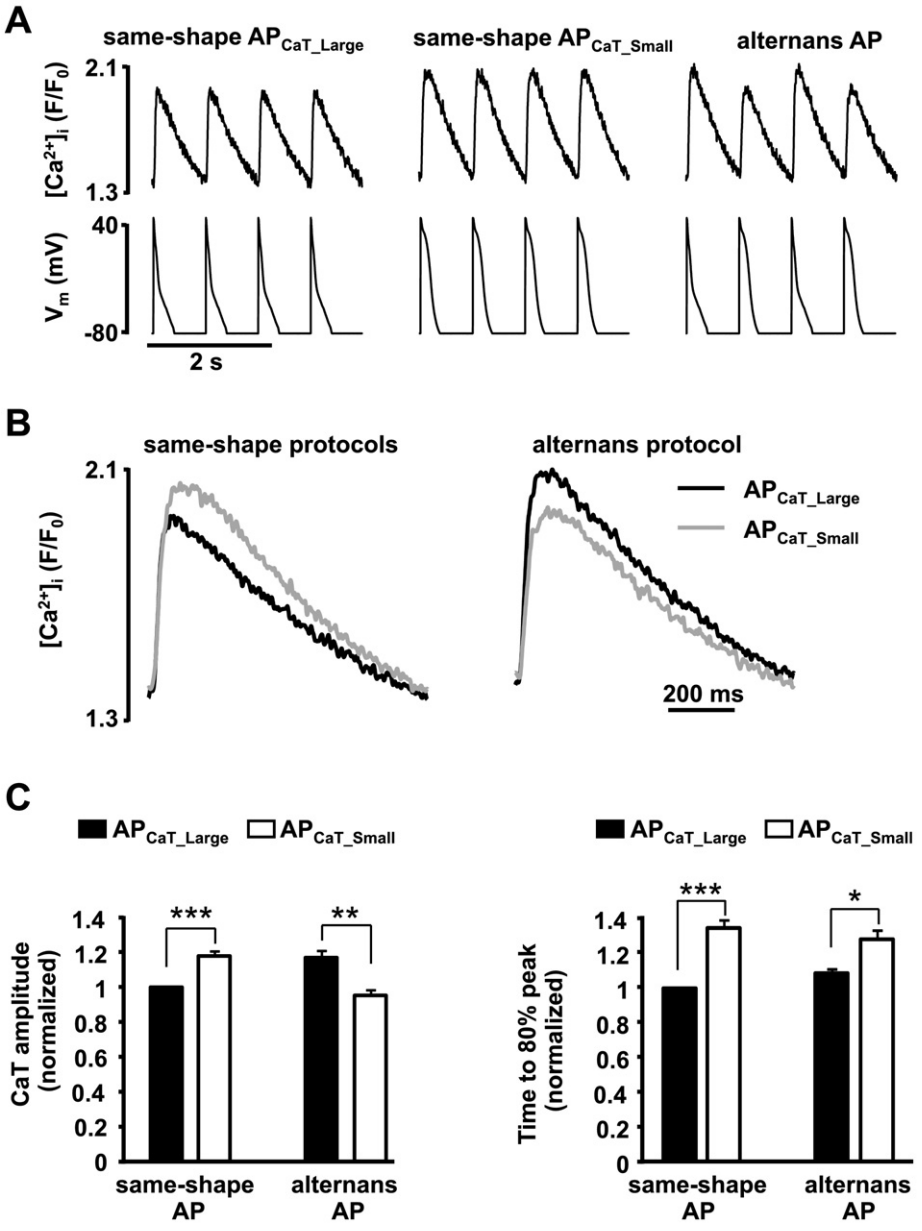

Fig. 2. Effect of AP morphology on CaTs properties. A, CaTs (top) elicited with same-shape AP_{CaT_Large}, same-shape AP_{CaT_Small} and alternans AP-clamp protocols (bottom) recorded from the same atrial myocyte at 1.19 Hz stimulation frequency. B, Overlays of CaTs elicited with AP_{CaT_Large} and AP_{CaT_Small} voltage commands during same-shape and alternans AP clamp protocols. Traces represent average of three consecutive CaTs recorded from the same cell as in panel A. C, Summary data for amplitudes and time to 80% of peak of CaTs recorded during same-shape and alternans AP voltage clamp protocols. Data are normalized to CaTs elicited with same-shape AP_{CaT_Large} pacing protocol (n = 17). $^{*}p < 0.01$, $^{**}p < 0.005$, $^{***}p < 0.0005$.

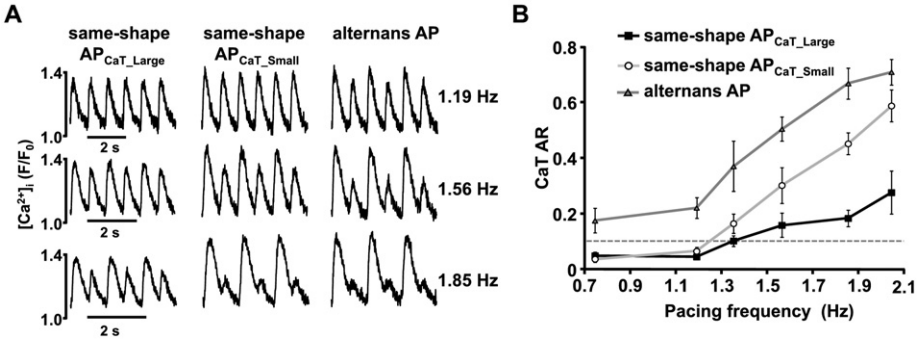

Fig. 3. AP waveforms modulate severity of CaT alternans. A, CaTs elicited with same-shape AP_{CaT_Large}, same-shape AP_{CaT_Small} and alternans AP clamp protocols recorded from the same atrial myocyte at different pacing frequencies. B, Pacing with same-shape AP_{CaT_Small} waveforms (open circles, n = 30) enhances degree of CaT alternans compared to AP_{CaT_Large} stimuli (black squares, n = 28). CaT alternans ratio (AR) is further increased during the alternans AP voltage clamp protocol (grey triangles, n = 18). Dashed line indicates definition of CaT alternans (AR > 0.1).

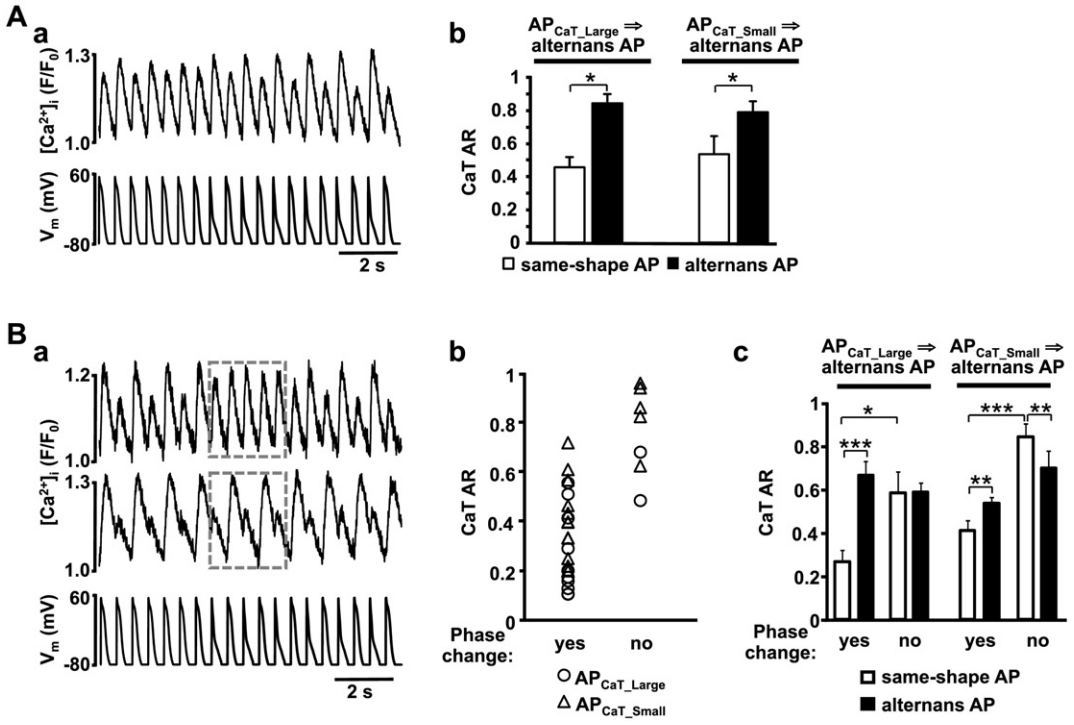

Fig. 4. In-phase and out-of-phase alternans during AP voltage clamp protocols. Same-shape AP voltage clamp protocols were followed by alternans AP voltage protocol. A, In-phase alternans. Aa, Example of sequence of same shape AP_{CaT_Small} voltage commands followed by alternans AP clamp protocol (bottom). CaT alternans are in-phase at the switch to the alternans AP clamp protocol and remain in-phase (top). Ab, average CaT ARs observed during stimulation with same-shape AP voltage commands (left: AP_{CaT_Large}; right: AP_{CaT_Small}) followed by alternans AP clamp protocol. Data refer only to the cells that are in-phase at the transition to the alternans protocol. B, Out-of-phase alternans. Ba, Examples of CaT alternans that are out-of-phase at the switch to the alternans AP clamp protocol, which leads either to a phase shift to in-phase (top) or remains out-of-phase (middle). Bottom: voltage clamp protocol. Bb, in the majority of cases a phase shift to in-phase occurred when the cell entered the alternans protocol out-of-phase, irrespective whether the preceding same-shape protocol consisted of AP_{CaT_Large} (circles) or AP_{CaT_Small} (triangles). The ability to change phase was determined by the degree of CaT alternans. Cells exhibiting CaT ARs lower than ~0.6 during the same-shape AP protocols were capable to reverse CaT alternans phase, while cells with higher CaT AR were not likely to change phase. Bc, Change of phase during alternans AP protocol resulted in increased AR. When CaTs alternans remained out-of-phase to AP alternans, no change or a decrease in AR was observed. Data is obtained from a total of 17 myocytes. *$p < 0.05$, **$p < 0.01$, ***$p < 0.0005$.

possibilities of alternans phase using a protocol where the same-shape $AP_{CaT\text{-}Small}$ protocol is followed by the alternans AP clamp protocol. Fig. 4A demonstrates the situation when the cell entered the alternans AP clamp phase "in-phase". In this case alternans remained in-phase during the entire alternans AP clamp protocol and increase in AR was observed (Fig. 4Ab). The same behavior was found when cells entered the alternans AP clamp period in-phase, but from a same-shape $AP_{CaT\text{-}Large}$ protocol (no traces shown, but summarized in Fig. 4Ab). However, when the cell entered the alternans AP clamp protocol "out-of-phase" two different patterns were observed: either the CaT alternans remained out-of-phase (Fig. 4Ba middle trace) or the cell underwent a phase shift and reverted to in-phase over the course of several beats (Fig. 4Ba upper trace). These two possibilities were observed irrespective whether the alternans AP clamp protocol was preceded by the same shape AP_{CaT_Small} (illustrated in Fig. 4Ba) or by the same shape AP_{CaT_Large} (no example shown) protocol. The ability of the cell to reverse CaT alternans phase correlated with degree of CaT alternans. Fig. 4Bb shows ARs from individual cells during the same shape AP clamp protocol (same shape AP_{CaT_Large} protocol: open circles; same shape AP_{CaT_Small} protocol: open triangles) that entered the alternans AP clamp protocol out-of-phase and subsequently underwent a phase shift (left panel) or remained out-of-phase (right panel). Fig. 4Bc shows average ARs during both periods of the protocol for the different scenarios: the mean CaT ARs during the initial same-shape AP clamp protocol for the population of cells that changed phase were 0.26 ± 0.05 ($n = 10$) for the AP_{CaT_Large} and 0.41 ± 0.05 ($n = 12$) for the AP_{CaT_Small} protocol, respectively. This group further revealed a significant AR increase during the subsequent alternans AP clamp protocol. The cells that failed to change the phase exhibited significantly higher AR during the initial same-shape AP protocol pacing: 0.58 ± 0.10 ($p < 0.05$) and 0.84 ± 0.06 ($p < 0.0005$) for AP_{CaT_Large} and AP_{CaT_Small}, respectively. In this case the AR remained constant or even decreased during the subsequent alternans AP clamp protocol.

In summary, data shown in Fig. 4 revealed a genuine tendency to retain or reestablish an in-phase pattern of AP and CaT alternans. When cells entered the alternans AP clamp protocol in-phase, alternans remained in-phase and no change in phase was observed. A phase shift was only observed when cells entered the alternans clamp protocol out-of-phase, and only remained out-of-phase when the CaT AR was already sufficiently high at that point.

3.3. AP morphology modulates sarcoplasmic reticulum Ca^{2+} load

In Fig. 2 we demonstrated a relationship between AP morphology and CaT magnitude, where during the same-shape AP clamp protocols larger CaTs are elicited by the AP_{CaT_Small} waveform compared to AP_{CaT_Large}, but this AP-CaT relationship reversed during the alternans AP clamp protocol. Thus, these observations suggest that the properties of CaTs are influenced by the AP morphology of the preceding beat. Since the magnitude of a CaT is strongly dependent on the availability of releasable Ca^{2+} from the SR, we tested the hypothesis that AP morphology directly affected SR Ca^{2+} load. We explored the relationship between AP shape and SR Ca^{2+} load by different complimentary approaches. First, $[Ca^{2+}]_{SR}$ was directly measured with the low affinity Ca-sensing dye Fluo-5N entrapped in the SR (Fig. 5A). The data show that end-diastolic $[Ca^{2+}]_{SR}$ was elevated when myocytes were paced with same-shape AP_{CaT_Small} protocol compared to the same-shape AP_{CaT_Large} protocol. In addition, beat-to-beat alternations in end-diastolic $[Ca^{2+}]_{SR}$ were observed during the alternans AP protocol. Here, the lower end-diastolic $[Ca^{2+}]_{SR}$ before an AP_{CaT_Small} was followed by

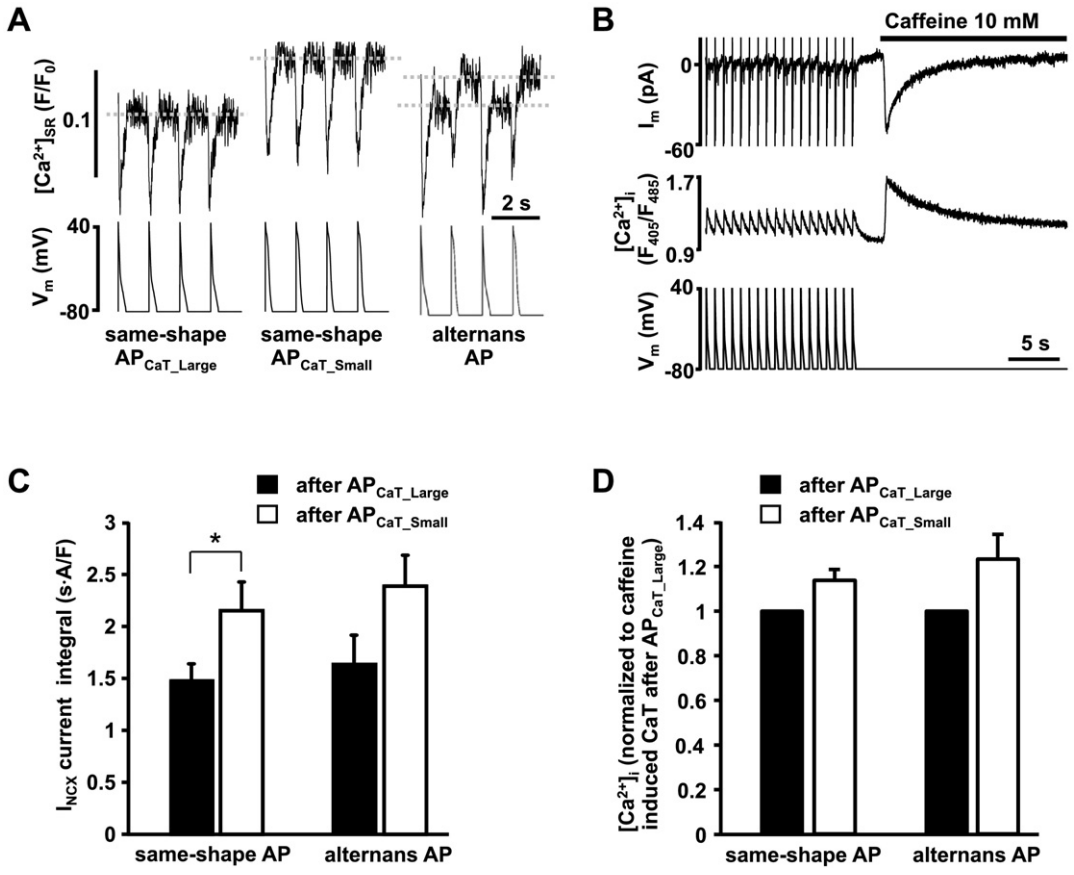

Fig. 5. AP morphology affects SR Ca^{2+} load. A, $[Ca^{2+}]_{SR}$ measurements with Fluo-5N from voltage clamped myocytes. The same myocyte was exposed to three different AP clamp protocols. End-diastolic $[Ca^{2+}]_{SR}$ was higher during the same-shape AP_{CaT_Small} protocol compared to AP_{CaT_Large} and revealed $[Ca^{2+}]_{SR}$ alternans during the alternans AP clamp protocol. B, Simultaneous membrane current (top) and $[Ca^{2+}]_i$ (middle) recording from an AP voltage clamped myocyte using the same-shape AP_{CaT_Large} protocol (bottom), followed by rapid application of caffeine (10 mM). C, SR Ca^{2+} load estimated from the integral of the membrane current induced by caffeine and representing extrusion of Ca^{2+} released from the SR via NCX. Caffeine was applied after pacing with same-shape AP_{CaT_Large} (n = 7), same-shape AP_{CaT_Small} (n = 7) and alternans AP voltage clamp (n = 6) protocols. D, SR Ca^{2+} load estimated from the normalized amplitudes of the cytosolic CaTs elicited with caffeine using the same protocols as in panel C. SR Ca^{2+} load was consistently higher after AP_{CaT_Small}. $^{*}p < 0.05$.

a smaller depletion amplitude during AP_{CaT_Small} resulting in a small amplitude cytosolic CaT (Fig. 2). To confirm the Fluo-5N results, we also determined SR Ca^{2+} load by measuring the cytosolic CaT amplitude elicited by rapid application of caffeine (10 mM) and by quantifying the time integral of the NCX current recorded during caffeine application (Fig. 5B). NCX current integral (Fig. 5C) and CaT amplitude (Fig. 5D) were measured immediately after cell pacing with the same-shape AP_{CaT_Large}, same-shape AP_{CaT_Small} and the alternans AP clamp protocol (thereby distinguishing whether AP_{CaT_Large} or AP_{CaT_Small} was the last stimulus applied before caffeine exposure). These data are summarized in figures 5C and 5D and indicate that during pacing with same-shape or alternans AP protocols a higher SR load was reached when myocytes were stimulated with the AP_{CaT_Small} waveform before application of caffeine, consistent with the Fluo-5N measurements.

3.4. AP morphology determines kinetics of L-type Ca^{2+} current and the efficiency of Ca^{2+}-induced Ca^{2+} release

The data shown in Fig. 5 demonstrate a relationship between AP morphology and SR Ca^{2+} load, and based on the data from Figs. 2 and 5 alone, SR Ca^{2+} load could - at least qualitatively - explain cytosolic CaT alternans, along the line of studies that suggested SR Ca^{2+} load as an important player in the development of cardiac alternans [13,20,21]. However, our results shown in Fig. 6 demonstrate that AP morphology additionally modulates CaTs by a mechanism independent of changes in $[Ca^{2+}]_{SR}$. In this series of experiments same-shape AP_{CaT_Large} and AP_{CaT_Small} protocols were used in sequence. It was consistently observed that the first CaT elicited with AP_{CaT_Small} waveform following a sequence of AP_{CaT_Large} stimuli was significantly smaller than the preceding CaT (Fig. 6A). The opposite was true when cells were stimulated with a series of AP_{CaT_Small}, followed by the AP_{CaT_Large} sequence. In this case the CaT induced with the first AP_{CaT_Large} stimulus was significantly larger (Fig. 6B). This change in CaT amplitude cannot be explained by differences in $[Ca^{2+}]_{SR}$, as Ca^{2+} available for release from SR is determined by the preceding pulses. Therefore, assuming that during cell stimulation with the same-shape protocol a steady-state Ca^{2+} loading of the SR is reached, the amount of Ca^{2+} available for release at the first AP-command of different shape is the same as for the preceding AP stimulation. Consequently, it can be concluded that for a given $[Ca^{2+}]_{SR}$ the AP_{CaT_Large} waveform is more efficient in triggering SR Ca^{2+} release.

It has been suggested that AP morphology affects L-type Ca^{2+} channels and modifies excitation-contraction coupling (ECC) in ventricular myocytes [22,23]. Therefore, we tested the hypothesis that the AP waveform determined magnitude and kinetics of I_{LCC} and thus the efficiency of the trigger of Ca^{2+}-induced Ca^{2+} release (CICR). Typical traces of I_{LCC} recorded during AP_{CaT_Large} and AP_{CaT_Small} in the absence of CaT alternans from the same atrial myocyte are shown in Fig. 7A. The AP_{CaT_Large} voltage protocols elicited I_{LCC} of larger magnitude but faster inactivation compared to I_{LCC} induced with the AP_{CaT_Small} voltage command (Fig. 7B). The duration of I_{LCC} (measured at 80% inactivation) was 87 ± 3 ms (n = 6) elicited by AP_{CaT_Large}, and 239 ± 23 ms (n = 6) for AP_{CaT_Small} (Fig. 7Ba). The mean peak I_{LCC} (measured as the peak

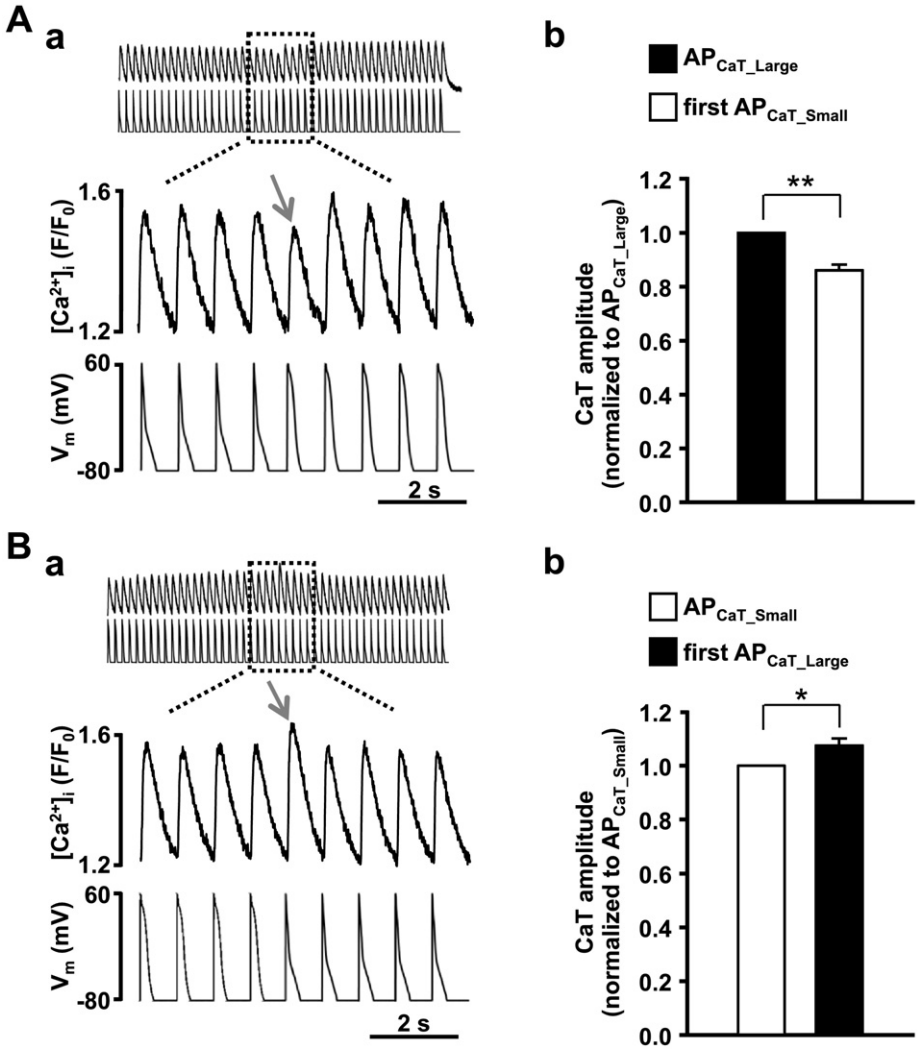

Fig. 6. AP_{CaT_Large} and AP_{CaT_Small} waveforms differ in CaT triggering efficiency. Aa, In the absence of CaT alternans, when the same-shape AP_{CaT_Large} protocol is followed by the same-shape AP_{CaT_Small} protocol the CaT transient elicited by the first AP_{CaT_Small} stimulus (indicated by the arrow) exhibits a decreased amplitude. Ab, Summary data of CaT amplitudes during initial stimulation with same-shape AP_{CaT_Large} protocol and the first CaTs after the switch of protocol to AP_{CaT_Small} ($n = 17$). Data are normalized to the CaT amplitudes observed during the initial stimulation with same-shape AP_{CaT_Large}. Ba, When same-shape AP_{CaT_Small} protocol is followed by the same-shape AP_{CaT_Large} protocol, the first AP_{CaT_Large} command elicits CaT of larger amplitude (indicated by the arrow). Bb, Summary data of CaT amplitudes during initial stimulation with same-shape AP_{CaT_Small} protocol and the first CaT elicited with AP_{CaT_Large} ($n = 16$). Data are normalized to the CaT amplitudes during same-shape AP_{CaT_Small} protocol. *$p < 0.05$, **$p < 0.0001$.

amplitude of the nifedipine (100 μM) sensitive current) was 2.4 ± 0.4 and 1.3 ± 0.2 pA/pF for AP_{CaT_Large} and AP_{CaT_Small}, respectively ($n = 6$). However, the net Ca^{2+} influx into the cell, estimated from the integral of I_{LCC}, was essentially identical during both voltage commands (Fig. 7Bb). The data show that AP_{CaT_Large} elicits an I_{LCC} that is more efficient as trigger of CICR. Thus, AP morphology determines I_{LCC} and CICR

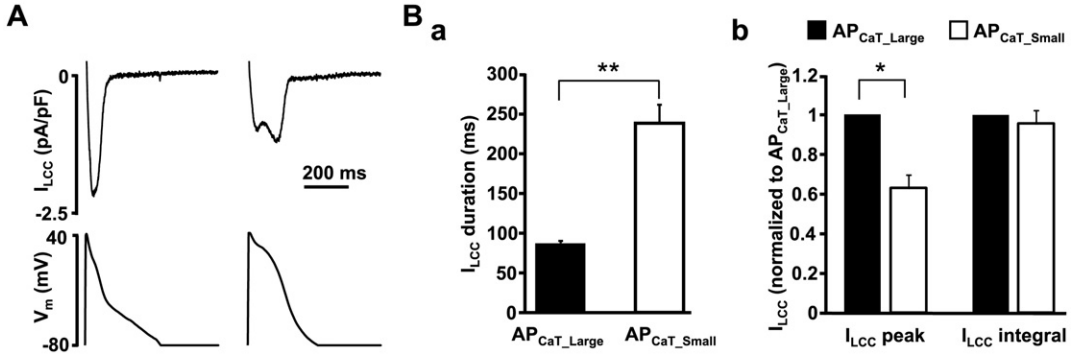

Fig. 7. AP alternans determines magnitude and kinetics of L-type Ca^{2+} current. A, Representative traces of I_{LCC} elicited with AP_{CaT_Large} and AP_{CaT_Small} voltage commands from the same atrial myocyte paced at 0.7 Hz (no CaT alternans). B, Summary data of I_{LCC} kinetics: duration of I_{LCC} measured at 80% inactivation of peak current (Ba; $n = 6$), and (Bb) average peak I_{LCC} and I_{LCC} time integrals elicited with AP_{CaT_Large} and AP_{CaT_Small} waveforms and normalized to AP_{CaT_Large} ($n = 6$). *$p < 0.05$, **$p < 0.0001$.

trigger efficiency and the beat-to-beat alternations of I_{LCC} in turn contribute to CaT alternans.

4. Discussion

In this study we investigated the effect of beat-to-beat alternations in AP morphology on the development of CaT alternans in rabbit atrial myocytes. The main findings are: i) pacing-induced CaT alternans were paralleled by electrical alternans characterized by distinct AP morphologies coinciding with the large and small amplitude CaTs (AP_{CaT_Large} and AP_{CaT_Small} measured under current clamp conditions); ii) AP clamp experiments applying various combinations of AP_{CaT_Large} and AP_{CaT_Small} command voltage protocols revealed that AP morphology determined pacing frequency threshold and degree of CaT alternans (AR), where iii) the latter was a dual effect of AP morphology on the efficiency of I_{LCC} as the trigger of CICR and on SR Ca^{2+} load.

4.1. Putative mechanisms of cardiac alternans

In cardiac myocytes electrical, mechanical and Ca^{2+} alternans are strongly correlated [8,9,24,25]. Beat-to-beat regulation of $[Ca^{2+}]_i$ and V_m is bi-directionally coupled with complex feedback mechanisms between these two parameters. Disturbances of this relationship are considered to cause electromechanical and CaT alternans [10,26,27].

Early studies have focused on AP restitution as an underlying mechanism of cardiac alternans [28,29]. By this hypothesis at high pacing frequency shortening of the diastolic interval leads to incomplete recovery of ion currents and therefore to beat-to-beat alternation in AP duration (APD). APD alternans then results in CaT alternans due to V_m-dependent regulation of Ca^{2+} influx through L-type Ca^{2+} channels and Ca^{2+} extrusion via NCX. However, more recent findings that CaT alternans can be elicited in voltage-clamped myocytes in the absence of beat-to-beat alternans in V_m [8,15,16,30,31] and therefore in the absence of AP alternans, support the alternative hypothesis that disturbances of intracellular Ca^{2+} handling is the primary cause of alternans. CaT alternans results in AP alternans by the activity of Ca^{2+}-regulated ion conductances such as NCX [32,33], L-type Ca^{2+} [32], Ca^{2+}-activated chloride [30], small conductance Ca^{2+}-activated K^+ channel currents [34]. A popular candidate for the underlying mechanism for CaT alternans was beat-to-beat fluctuations in SR Ca^{2+} load [13,20,21], however others have demonstrated that CaT alternans could be observed without alternans in diastolic $[Ca^{2+}]_{SR}$ [25,35]. As an alternative to the SR Ca^{2+} load hypothesis, beat-to-beat differences in refractoriness of SR Ca^{2+} release was suggested [14,36–38].

The importance of V_m in alternans development was primarily suggested by simulation studies [17–19], but had scarce experimental support. Without challenging the general notion that the primary defect leading to cardiac alternans resides in Ca^{2+} signaling disturbances, in the present study we provide new experimental evidence that beat-to-beat alternation in AP morphology plays an important role in the sustainability and degree of CaT alternans.

4.2. The role of AP morphology in the development of CaT alternans

In rabbit atrial myocytes pacing-induced CaT and AP alternans are strongly correlated and distinctive AP waveforms coincide with large and small CaTs [8]. APs recorded with the current clamp technique (Fig. 1) during large amplitude alternans CaT exhibited a faster repolarization rate, were significantly shorter at 30% repolarization and slightly prolonged at 90% repolarization level [8]. These characteristic AP waveforms during CaT alternans were used to generate different voltage command sequences for AP clamp experiments aimed at experimentally emulate V_m changes during AP alternans. The results strongly suggest that AP morphology and beat-to-beat alternation in AP shape play a very important role in the regulation of intracellular Ca^{2+} handling and consequently the phenotype of CaT alternans. This conclusion is based on the following observations: (a) while previous studies have emphasized the role of disturbances in Ca^{2+} handling and have demonstrated CaT alternans in the absence of V_m alternans [8,15,16], here we demonstrate that beat-to-beat alternations in AP morphology can induce CaT alternans at lower pacing rates where CaT alternans are not observed when beat-to-beat AP morphology was kept constant (Figs. 2 and 3A). (b) The alternans AP-clamp protocol induced CaT alternans of higher degree (higher AR; Fig. 3) than the same-shape AP clamp protocols. (c) Applying a same-shape AP clamp protocol, for any given pacing frequency the AP_{CaT_Small} waveform induced more pronounced CaT alternans with higher AR compared to the AP_{CaT_Large} protocol, underscoring the importance of AP morphology for the generation of CaT alternans (Fig. 3). (d) CaT alternans have a strong tendency to be "in-phase", i.e. during alternans AP clamp the AP_{CaT_Large} voltage command usually elicits large CaT. When cells are 'forced' into "out-of-phase" conditions cells typically revert to an in-phase pattern. Only when CaT alternans is very pronounced (high AR) the out-of-phase pattern prevails (Fig. 4).

4.3. Alternation in AP morphology determines beat-to-beat variations in SR Ca^{2+} load during CaT alternans

While a positive correlation between APD and SR Ca^{2+} load is well known [23,39] it has not been shown experimentally under alternans conditions. Here we present new experimental evidence that the changes in AP morphology during alternans affect diastolic SR Ca^{2+} load to the extent that it has direct consequences for the development of CaT alternans. By measuring $[Ca^{2+}]_{SR}$ directly and dynamically with the SR entrapped low affinity Ca^{2+} probe Fluo-5N (Fig. 5A) we observed end-diastolic $[Ca^{2+}]_{SR}$ alternans during alternans AP clamp conditions. Measuring cytosolic CaTs and NCX currents elicited with rapid caffeine applications under alternans AP clamp conditions confirmed the Fluo-5N results (Fig. 5B-D). In addition, AP morphology determined properties of CaT and end-diastolic $[Ca^{2+}]_{SR}$ even at pacing frequencies below the CaT alternans threshold. The same-shape AP clamp protocol using the AP_{CaT_Small} waveform consistently induced CaTs of larger magnitude and led to higher end-diastolic $[Ca^{2+}]_{SR}$ than the same-shape AP_{CaT_Large} clamp protocol. This AP shape-CaT magnitude relationship was however reversed during alternans AP clamp protocol where larger CaTs were elicited with AP_{CaT_Large} (Fig. 2). The data suggest that AP morphology modulates SR Ca^{2+} load and suggests that beat-to-beat alternations of end-diastolic $[Ca^{2+}]_{SR}$ constitutes a contributing factor to CaT alternans as suggested in the earlier studies [13,35]. However, the putative dependence of CaT alternans on AP morphology cannot be explained on the basis of SR Ca^{2+} load alone.

4.4. CaT alternans are modulated by AP morphology-dependent I_{LCC} kinetics and trigger efficiency of CICR

An important finding of our study is the demonstration that AP morphology directly contributes to the development of alternans by determining ECC efficiency. At constant beat-to-beat $[Ca^{2+}]_{SR}$ the AP_{CaT_Large} waveform is a more efficient trigger for CICR than AP_{CaT_Small} (Fig. 6). Previously, Sah et al. [23,40] showed that ECC is affected by the AP repolarization rate in rat ventricular myocytes and this effect was attributed to the modulation of Ca^{2+} influx through LCCs. We report similar findings here in rabbit atrial myocytes and we demonstrate that AP morphology during alternans determines amplitude and kinetics of I_{LCC} (Fig. 7). I_{LCC} elicited with AP_{CaT_Large} exhibits a larger amplitude and therefore is more efficient in triggering CICR (Fig. 7B), despite the fact that the total Ca^{2+} influx into the cell (estimated from integration of total I_{LCC} during the AP) is virtually identical for both AP waveforms. Thus, the amount of Ca^{2+} entering the cell during both AP_{CaT_Large} and AP_{CaT_Small} are the same, and therefore the increased $[Ca^{2+}]_{SR}$ during pacing with AP_{CaT_Small} (Fig. 5) cannot be attributed to an increased Ca^{2+} entry. However, changes in SR Ca^{2+} load can be, at least partially,

explained by the AP-morphology dependent CaT triggering efficiency - i.e. the AP_{CaT_SmalI} waveform elicits an I_{LCC} of smaller amplitude that is less efficient in triggering SR release. Consequence of a smaller SR Ca^{2+} release is a higher $[Ca^{2+}]_{SR}$ available for the next beat. Taken together, the data suggest that AP morphology during CaT alternans determines the efficiency of CICR mediated by peak I_{LCC} and secondarily leads to beat-to-beat fluctuations of $[Ca^{2+}]_{SR}$ which in turn stabilizes and potentially enhances the degree of CaT alternans.

4.5. Summary and outlook

To date the vast majority of the studies focusing on cardiac alternans mechanisms were performed on ventricular tissue, despite the established notion that atrial alternans is causally linked to atrial fibrillation, the most frequent cardiac arrhythmia [1–4]. Notwithstanding similarities, atrial and ventricular cells exhibit significant differences in both intracellular Ca^{2+} handling and plasmalemmal ion channel expression [41,42]. This study provides new insights into alternans mechanisms in the atrium. While the importance of the bi-directional coupling between V_m and Ca^{2+} for the development of cardiac alternans is widely accepted and cannot be stressed enough, recently the attention has shifted to instabilities in cellular Ca^{2+} hand-ling as the cause of alternans, leaving the role of V_m instabilities increasingly neglected. This study provides new evidence that alternation in V_m and AP morphology plays a significant role in the development and stabilization of atrial alternans. We established two mechanisms by which V_m contributes to CaT alternans: 1) changes in SR Ca^{2+} load and 2) modulation of I_{LCC} which determines the efficiency of ECC. AP prolongation and beat-to-beat alternation in AP morphology both contribute to the development and degree of CaT alternans. The demonstration that CaT alternans can be controlled or even prevented by modulating AP morphology has important ramifications in light of arrhythmia prevention and therapy strategies. A wide array of pharmacological modulators of ion channels - many already in clinical use - could be applied with the specific target to alter the AP into a desirable morphology that correlates with a low probability to induce Ca^{2+} alternans.

Sources of funding

This work was supported by National Institutes of Health grants HL057832, HL080101, and HL101235 and the Fondation Leducq (to L.A.B.). G.K. was supported by a Rush Translational Sciences Consortium Schweppe and Armour Award for Young Investigators and American Heart Association grant 16GRNT30130011.

Disclosures

None.

References

[1] P. Comtois, S. Nattel, Atrial repolarization alternans as a path to atrial fibrillation, J. Cardiovasc. Electrophysiol. 23 (2012) 1013–1015.
[2] K. Hiromoto, H. Shimizu, Y. Furukawa, T. Kanemori, T. Mine, T. Masuyama, et al., Discordant repolarization alternans-induced atrial fibrillation is suppressed by verapamil, Circ. J. 69 (2005) 1368–1373.
[3] S.M. Narayan, F. Bode, P.L. Karasik, M.R. Franz, Alternans of atrial action potentials during atrial flutter as a precursor to atrial fibrillation, Circulation 106 (2002) 1968–1973.
[4] F. Jousset, J. Tenkorang, J.M. Vesin, P. Pascale, P. Ruchat, A.G. Rollin, et al., Kinetics of atrial repolarization alternans in a free-behaving ovine model, J. Cardiovasc. Electrophysiol. 23 (2012) 1003–1012.
[5] M.L. Walker, D.S. Rosenbaum, Repolarization alternans: implications for the mechanism and prevention of sudden cardiac death, Cardiovasc. Res. 57 (2003) 599–614.
[6] M.L. Walker, D.S. Rosenbaum, Cellular alternans as mechanism of cardiac arrhythmogenesis, Heart Rhythm. 2 (2005) 1383–1386.
[7] H.E. Ter Keurs, P.A. Boyden, Calcium and arrhythmogenesis, Physiol. Rev. 87 (2007) 457–506.
[8] G. Kanaporis, L.A. Blatter, The mechanisms of calcium cycling and action potential dynamics in cardiac alternans, Circ. Res. 116 (2015) 846–856.
[9] E.J. Pruvot, R.P. Katra, D.S. Rosenbaum, K.R. Laurita, Role of calcium cycling versus restitution in the mechanism of repolarization alternans, Circ. Res. 94 (2004) 1083–1090.
[10] J.N. Weiss, A. Karma, Y. Shiferaw, P.S. Chen, A. Garfinkel, Z. Qu, From pulsus to pulseless: the saga of cardiac alternans, Circ. Res. 98 (2006) 1244–1253.
[11] J.N. Edwards, L.A. Blatter, Cardiac alternans and intracellular calcium cycling, Clin. Exp. Pharmacol. Physiol. 41 (2014) 524–532.
[12] J.I. Goldhaber, L.H. Xie, T. Duong, C. Motter, K. Khuu, J.N. Weiss, Action potential duration restitution and alternans in rabbit ventricular myocytes: the key role of intracellular calcium cycling, Circ. Res. 96 (2005) 459–466.
[13] M.E. Diaz, S.C. O'Neill, D.A. Eisner, Sarcoplasmic reticulum calcium content fluctuation is the key to cardiac alternans, Circ. Res. 94 (2004) 650–656.
[14] V.M. Shkryl, J.T. Maxwell, T.L. Domeier, L.A. Blatter, Refractoriness of sarcoplasmic reticulum Ca^{2+} release determines Ca^{2+} alternans in atrial myocytes, Am. J. Physiol. Heart Circ. Physiol. 302 (2012) H2310–H2320.
[15] E. Chudin, J. Goldhaber, A. Garfinkel, J. Weiss, B. Kogan, Intracellular Ca^{2+} dynamics and the stability of ventricular tachycardia, Biophys. J. 77 (1999) 2930–2941.
[16] X. Wan, K.R. Laurita, E.J. Pruvot, D.S. Rosenbaum, Molecular correlates of repolarization alternans in cardiac myocytes, J. Mol. Cell. Cardiol. 39 (2005) 419–428.
[17] P.N. Jordan, D.J. Christini, Action potential morphology influences intracellular calcium handling stability and the occurrence of alternans, Biophys. J. 90 (2006) 672–680.
[18] P.N. Jordan, D.J. Christini, Characterizing the contribution of voltage- and calcium-dependent coupling to action potential stability: implications for repolarization alternans, Am. J. Physiol. Heart Circ. Physiol. 293 (2007) H2109–H2118.
[19] Y. Shiferaw, D. Sato, A. Karma, Coupled dynamics of voltage and calcium in paced cardiac cells, Phys. Rev. E Stat. Nonlinear Soft Matter Phys. 71 (2005) 021903.
[20] D.A. Eisner, Y. Li, S.C. O'Neill, Alternans of intracellular calcium: mechanism and significance, Heart Rhythm. 3 (2006) 743–745.
[21] M. Nivala, Z. Qu, Calcium alternans in a coupon network model of ventricular myocytes: role of sarcoplasmic reticulum load, Am. J. Physiol. Heart Circ. Physiol. 303 (2012) H341–H352.
[22] K.W. Linz, R. Meyer, Profile and kinetics of L-type calcium current during the cardiac ventricular action potential compared in guinea-pigs, rats and rabbits, Pflugers Arch. 439 (2000) 588–599.
[23] R. Sah, R.J. Ramirez, R. Kaprielian, P.H. Backx, Alterations in action potential profile enhance excitation-contraction coupling in rat cardiac myocytes, J. Physiol. 533 (2001) 201–214.
[24] H.C. Lee, R. Mohabir, N. Smith, M.R. Franz, W.T. Clusin, Effect of ischemia on calcium-dependent fluorescence transients in rabbit hearts containing Indo 1. Correlation with monophasic action potentials and contraction, Circulation 78 (1988) 1047–1059.
[25] J. Huser, Y.G. Wang, K.A. Sheehan, F. Cifuentes, S.L. Lipsius, L.A. Blatter, Functional coupling between glycolysis and excitation-contraction coupling underlies alternans in cat heart cells, J. Physiol. 524 (Pt 3) (2000) 795–806.
[26] W.T. Clusin, Mechanisms of calcium transient and action potential alternans in cardiac cells and tissues, Am. J. Physiol. Heart Circ. Physiol. 294 (2008) H1–H10.
[27] S.A. Gaeta, D.J. Christini, Non-linear dynamics of cardiac alternans: subcellular to tissue-level mechanisms of arrhythmia, Front. Physiol. 3 (2012) 157.
[28] J.B. Nolasco, R.W. Dahlen, A graphic method for the study of alternation in cardiac action potentials, J. Appl. Physiol. 25 (1968) 191–196.
[29] J.J. Fox, J.L. McHarg, R.F. Gilmour Jr., Ionic mechanism of electrical alternans, Am. J. Physiol. Heart Circ. Physiol. 282 (2002) H516–H530.
[30] G. Kanaporis, L.A. Blatter, Calcium-activated chloride current determines action potential morphology during calcium alternans in atrial myocytes, J. Physiol. 594 (2016) 699–714.
[31] G. Kanaporis, L.A. Blatter, Ca^{2+}-activated chloride channel activity during Ca^{2+} alternans in ventricular myocytes, Channels (Austin) 10 (2016) 507–517.
[32] X. Zhou, A. Bueno-Orovio, M. Orini, B. Hanson, M. Hayward, P. Taggart, et al., In vivo and in silico investigation into mechanisms of frequency dependence of repolarization alternans in human ventricular cardiomyocytes, Circ. Res. 118 (2016) 266–278.
[33] X. Wan, M. Cutler, Z. Song, A. Karma, T. Matsuda, A. Baba, et al., New experimental evidence for mechanism of arrhythmogenic membrane potential alternans based on balance of electrogenic I(NCX)/I(Ca) currents, Heart Rhythm. 9 (2012) 1698–1705.
[34] C.H. Hsueh, P.C. Chang, Y.C. Hsieh, T. Reher, P.S. Chen, S.F. Lin, Proarrhythmic effect of blocking the small conductance calcium activated potassium channel in isolated canine left atrium, Heart Rhythm. 10 (2013) 891–898.
[35] E. Picht, J. DeSantiago, L.A. Blatter, D.M. Bers, Cardiac alternans do not rely on diastolic sarcoplasmic reticulum calcium content fluctuations, Circ. Res. 99 (2006) 740–748.
[36] C.A. Lugo, I.R. Cantalapiedra, A. Penaranda, L. Hove-Madsen, B. Echebarria, Are SR Ca content fluctuations or SR refractoriness the key to atrial cardiac alternans?: insights from a human atrial model, Am. J. Physiol. Heart Circ. Physiol. 306 (2014) H1540–H1552.
[37] L. Wang, R.C. Myles, N.M. De Jesus, A.K. Ohlendorf, D.M. Bers, C.M. Ripplinger, Optical mapping of sarcoplasmic reticulum Ca^{2+} in the intact heart: ryanodine receptor refractoriness during alternans and fibrillation, Circ. Res. 114 (2014) 1410–1421.
[38] D. Kornyeyev, A.D. Petrosky, B. Zepeda, M. Ferreiro, B. Knollmann, A.L. Escobar, Calsequestrin 2 deletion shortens the refractoriness of Ca^{2+} release and reduces rate-dependent Ca^{2+}-alternans in intact mouse hearts, J. Mol. Cell. Cardiol. 52 (2012) 21–31.

[39] R.A. Bassani, J. Altamirano, J.L. Puglisi, D.M. Bers, Action potential duration determines sarcoplasmic reticulum Ca^{2+} reloading in mammalian ventricular myocytes, J. Physiol. 559 (2004) 593–609.
[40] R. Sah, R.J. Ramirez, G.Y. Oudit, D. Gidrewicz, M.G. Trivieri, C. Zobel, et al., Regulation of cardiac excitation-contraction coupling by action potential repolarization: role of the transient outward potassium current (I_{to}), J. Physiol. 546 (2003) 5–18.
[41] D. Tuteja, D. Xu, V. Timofeyev, L. Lu, D. Sharma, Z. Zhang, et al., Differential expression of small-conductance Ca^{2+}-activated K^+ channels SK1, SK2, and SK3 in mouse atrial and ventricular myocytes, Am. J. Physiol. Heart Circ. Physiol. 289 (2005) H2714–H2723.
[42] H. Dobrzynski, D.D. Marples, H. Musa, T.T. Yamanushi, Z. Henderson, Y. Takagishi, et al., Distribution of the muscarinic K^+ channel proteins Kir3.1 and Kir3.4 in the ventricle, atrium, and sinoatrial node of heart, J. Histochem. Cytochem. 49 (2001) 1221–1234.